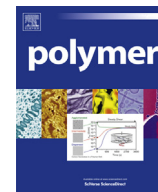


Contents lists available at [SciVerse ScienceDirect](http://www.sciencedirect.com)

Polymer

journal homepage: www.elsevier.com/locate/polymer

Influence of ionic liquid on selective polycondensation of a new diamine-bisphenol: Synthesis and properties of polyamides and their composites with modified nanosilica

Mehdi Taghavi, Mousa Ghaemy*, Seyed Mojtaba Amini Nasab, Marjan Hassanzadeh

Polymer Chemistry Research Laboratory, Department of Chemistry, University of Mazandaran, Babolsar 47416-95447, Iran

ARTICLE INFO

Article history:

Received 20 February 2013

Received in revised form

30 April 2013

Accepted 5 May 2013

Available online xxx

Keywords:

Ionic liquids

Polyamide

Nanocomposite

ABSTRACT

This work reports that imidazolium-based ionic liquids (ILs) are very efficient solvents and catalysts for the selective synthesis of novel high performance polyamides (PAs) from a new diamine-bisphenol. Direct polycondensation of the diamine-bisphenol was carried out with various dicarboxylic acids by using mixture of: (1) triphenylphosphite (TPP)/*N*-methylpyrrolidone (NMP)/pyridine (Py)/LiCl; and (2) IL/TPP. The PAs were obtained in no more than 2.5 h at 110 °C, which is considerably shorter than the conventional direct polycondensation, with mass-average molar mass (M_w) up to 61,000 g mol⁻¹, glass transition temperatures (T_g) up to 325 °C and 10% weight loss temperatures ($T_{10\%}$) up to 511 °C (in N₂) and 456 °C (in air). Nanocomposites of these PAs with modified nanosilica (mNS) showed that strong chemical bonding between inorganic particles and the polymer matrix contributed to the enhanced thermal and mechanical properties. The photoluminescence intensity of the PAs increased and the spectra red shifted with increasing mNS content. The PAs and nanocomposites were tested for their extraction capability of metal ions such as Cr³⁺, Co²⁺, Zn²⁺, Pb²⁺, Cd²⁺, Hg²⁺ and Fe³⁺ from aqueous solutions either individually or in the mixture.

© 2013 Elsevier Ltd. All rights reserved.

1. Introduction

In recent years much attention has been given to reusability of solvents and catalysts for the development of cost-effective protocols [1]. Ionic liquids (ILs) are organic salts that are liquid at ambient temperatures and act much like good organic solvents dissolving both polar and nonpolar species [2,3]. Since the concept of green chemistry has emerged, much attention has been paid to organic chemistry processes involving ILs as non-volatile, easily recyclable reaction media of high thermal and chemical stabilities. These characteristics have made them as potential green solvents for preparing polymers with various polymerization mechanisms [4,5]. Most polycondensation studies were relative to the synthesis of aromatic polymers such as polyamides, polyimides, polyhydrazides or polyoxadiazoles in a range of conventional ionic liquids [6–9]. Polyamides (PAs) are one of the high-performance polymeric materials and are characterized by thermo oxidative stability, good mechanical properties, and outstanding solvent resistance [10–12]. However, because of difficulty in processing

aromatic PAs, many researchers have focused on development of structurally modified PAs with increased solubility and better processability through introducing bulky side groups [13–18] flexible units [19–21] and breaking symmetry and regularity of the polymer chain [22–24]. Organic-inorganic hybrid materials have been paid on much attention in the last decades due to the synergetic effect of organic and inorganic components in nanoscales. The combination of organic and inorganic components is expected to provide remarkable and complementary properties, which cannot be obtained with a single material [25–27]. Compared to composites containing larger dispersed particles, nanocomposites have the advantage of achieving the optimal properties at relatively low filler content, resulting in a lower density and better surface smoothness and transparency. The advantages in mechanical properties of nanocomposites, such as the higher modulus and yield stress, are usually accompanied by an increase in melt viscosity and a change in rheological behaviour [28–32]. In this paper, for the first time, synthesis and characterization of new polyamides from a tetrafunctional compound containing both –NH₂ and –OH groups is described. The PAs were synthesized selectively from the diamine-bisphenol compound in the mixture of IL/TPP without using Py/NMP/LiCl which is required in the conventional direct polycondensation. The PAs which were

* Corresponding author. Tel.: +98 112 5342353; fax: +98 112 5342350.

E-mail address: ghaemy@umz.ac.ir (M. Ghaemy).

obtained in IL and bearing reactive phenolic hydroxyl groups were used in preparation of composites chemically bounded with modified NS particles. The PAs and nanocomposites were characterized by using FT-IR, NMR, XRD and AFM techniques and their properties such as solubility, thermal, photophysical, mechanical and ability for removal of environmentally toxic heavy metal ions were investigated.

2. Experimental

2.1. Materials

All chemicals were purchased from Fluka and Merck Chemical Co. (Germany). Ammonium acetate, hydrazine monohydrate, 10% palladium on activated carbon, (3-chloropropyl)trimethoxysilane (CTMS), terephthalic acid, isophthalic acid, pyridine-2,6-dicarboxylic acid, 4,4'-sulfonyldibenzoic acid, adipic acid and sebacic acid were used as received. *N*-methyl-2-pyrrolidone (NMP), *N,N*-dimethylacetamide (DMAc), and pyridine (Py) were purified by distillation under reduced pressure over calcium hydride and stored over 4 Å molecular sieves. NS was purchased from Nissan Chemical Co. (Tokyo, Japan). Characteristic data for NS particles are absorption bands at 3397 and 1106 cm^{-1} related to hydroxyl and Si–O–Si groups, respectively. 4,4'-dihydroxy benzyl was synthesized and characterized recently in our research laboratory [23]. All ionic liquids were prepared by using previously reported procedure [33].

2.2. Measurements

Proton and carbon nuclear magnetic resonance (^1H NMR and ^{13}C NMR) spectra were recorded on a 400 MHz Bruker Avance DRX instrument (Germany) using DMSO- d_6 as solvent and tetramethyl silane as an internal standard. Proton resonances are designated as singlet (s), doublet (d), and multiplet (m). FT-IR spectra were recorded using a Bruker Tensor 27 spectrometer on KBr pellets over the range of 400–4000 cm^{-1} . Elemental analyses performed by a CHN-600 Leco elemental analyzer. Melting point (uncorrected) was measured with a Barnstead Electrothermal engineering LTD 9200 apparatus. Inherent viscosities (at a concentration of 0.5 g/dL) were measured with an Ubbelohde suspended-level viscometer at 25 °C using NMP as solvent. Quantitative solubility was determined using 0.05 g of a polymer in 0.5 mL of solvent. For the moisture absorption measurement, 200 mg polymer powder was dried at 120 °C for 8 h and then placed in an open space with a relative humidity of 80%. The samples were weighed periodically over the course of 48 h. The GPC measurements were conducted at 30 °C with a Perkin–Elmer instrument equipped with a differential refractometer detector. The columns used were packed with a polystyrene/divinylbenzene copolymer (PL gel MIXED-B from Polymer Laboratories) with DMF as fluent at a flow rate of 1 mL/min. Calibration of the instrument was done with monodisperse polystyrene standards. Thermogravimetric analysis (TGA) was performed with the DuPont Instruments (TGA 951) analyzer at a heating rate of 10 °C/min under N_2 (20 cm^3/min) and in air in temperature range of 30–650 °C. Differential scanning calorimeter (DSC) was recorded on a Perkin Elmer pyres 6 DSC under nitrogen atmosphere (20 cm^3/min) at a heating rate of 10 °C/min. Glass-transition temperatures (T_g) values were read at the middle of the transition in heat capacity and were taken from the second heating scan after cooling from 350 °C to room temperature (~30 °C) at a cooling rate of 20 °C min^{-1} . Ultraviolet-visible and fluorescence emission spectra were recorded on a Cecil 5503 (Cecil Instruments, Cambridge, UK) and Perkin–Elmer LS-3B spectrophotometers (Norwalk, CT, USA) (slit width = 2 nm), respectively, using a dilute polymer solution

(0.20 g/dL) in DMSO. To measure the photoluminescence (PL) quantum yields (Φ_f), dilute PAs solutions (0.2 g/dL) in NMP were prepared. A 0.10 N solution of quinine in H_2SO_4 ($\Phi_f = 0.53$) was used as a reference [33]. To prepare crack-free and homogeneous thin films for the measurement of optical properties, solutions were made by dissolving about 0.5 g of polymer in 5 mL DMF to afford an approximate 10 wt% solution. The homogeneous solution was poured into a 9 cm-diameter glass culture dish, heated under vacuum at 50 °C for 2 h, 100 °C for 5 h, and 150 °C for 3 h to evaporate the solvent slowly. Polymer films were self-stripped off from the glass surface by soaking in water. The polymer films were further dried in vacuum oven at 170 °C for 10 h. X-ray powder diffraction patterns were recorded by an X-ray diffractometer (GBC MMA instrument) with Be-filtered Cu K (1.5418 Å) operating at 35.4 kV and 28 mA. The 2θ scanning range was set between 4° and 50° at a scan rate of 0.05° pers . Atomic force microscopic (AFM) Easy Scan 2 Flex AFM (Swiss Co), was used to investigate the surface phase and topography of the nanocomposites. Branson S3200 (50 kHz, 150 W) ultrasonic bath was used for better dispersion of nanoparticles. To determine the tensile properties of the polymers, strips (5 mm in width and 30 mm in length) were cut from polymer films of 30–50 μm thickness on a MTS Criterion™ Universal Test Systems at 20 °C. Mechanical clamps were used and an extension rate of 5 mm min^{-1} was applied using a gauge length of 10 mm. At least six samples were tested for each polymer and the average values are reported. The solid–liquid extraction of Hg^{2+} , Cd^{2+} , Ni^{2+} , Co^{2+} , Cu^{2+} , Cr^{3+} and Fe^{3+} as their nitrate salts was carried out at pH = 7–8 from metal aqueous solutions either individually or in the mixture. Approximately 50 mg of the appropriate polymer powder was shaken with 50 mL of an aqueous solution of the metal salt for a week at 25 °C (equilibrium was assessed in less than three days). The initial concentration of salts was 20 mg L^{-1} . After filtration, the concentration of each metal cation in the liquid phase was determined by atomic absorption (BRAIC WFX-130 AA), and direct information regarding the extraction percentages of metal ions by polymers was obtained by using a calibration curve made from standard solutions of 5, 10, and 20 ppm for each metal salts.

2.3. Monomer synthesis

2.3.1. Synthesis of 2,4-bis(4-nitrophenoxy)benzaldehyde (1)

In a 500 mL round-bottomed two-necked flask equipped with a condenser, a magnetic stir bar and a nitrogen gas inlet tube, a mixture of 1.38 g (10 mmol) 2,4-dihydroxy benzaldehyde, 2.82 g (20 mmol) 1-fluoro-4-nitrobenzene, and 2.76 g (20 mmol) anhydrous potassium carbonate in 10 mL dry DMSO was refluxed at 120 °C for 12 h. After completion of the reaction (as witnessed by TLC test), the solution was cooled to room temperature. The reaction mixture was poured into 400 mL deionized water. The resulting yellowish powder was collected by filtration, washed with water repeatedly, dried in a vacuum oven and then recrystallization from ethanol. The yield of the reaction was 93% (3.55 g), and the melting point was 152–156 °C. FT-IR (KBr disk) at cm^{-1} : 3105 (C–H aromatic), 2842 (C–H aldehyde), 1684 (C=O aldehyde), 1583 (C=C), 1522, 1350 (NO_2) and 1229 (C–O–C). ^1H NMR (500 MHz, DMSO- d_6 , δ in ppm): 7.08 (d, 1H, Ar–H, $J = 2.1$ Hz), 7.19 (dd, 1H, Ar–H, $J = 8.0$ Hz), 7.29–7.38 (m, 4H, Ar–H), 8.03 (d, 1H, Ar–H, $J = 8.5$ Hz), 8.26–8.34 (m, 4H, Ar–H), 10.16 (s, 1H, C–H aldehyde). Elemental analysis calculated for $\text{C}_{19}\text{H}_{12}\text{N}_2\text{O}_7$: C, 60.00%; H, 3.18%; N, 7.37% and found: C, 59.98%; H, 3.25%; N, 7.32%.

2.3.2. Synthesis of 4,4'-(2-(2,4-bis(4-nitrophenoxy)phenyl)-1H-imidazole-4,5-diyl) diphenol (2)

In a 500 mL round-bottomed two-necked flask equipped with a condenser, a magnetic stir bar and a nitrogen gas inlet tube, a mixture

of 3.8 g (0.01 mol) 2,4-bis(4-nitrophenoxy)benzaldehyde, 2.1 g (0.01 mol) 4,4'-dihydroxy benzil, 2.42 g (0.07 mol) ammonium acetate and 50 mL glacial acetic acid was refluxed for 24 h. Upon cooling, the white precipitate was collected by filtration and washed with ethanol and water. The yield of the crude product was 5.5 g (91%). The crude product was recrystallized from ethanol to afford white solid with melting point 312–315 °C. FT-IR (KBr disk) at cm^{-1} : 3208–3550 (OH and NH imidazole), 3115 (C–H aromatic), 1615 (C=N), 1588 (C=C), 1521, 1352 (NO₂), 1266 and 1228 (C–O). ¹H NMR (DMSO-*d*₆, δ in ppm): 6.49 (dd, 1H, Ar–H, *J* = 8.2 Hz), 6.61 (d, 1H, Ar–H, *J* = 2.4), 6.68 (d, 2H, Ar–H, *J* = 8.4 Hz), 6.70 (d, 2H, Ar–H, *J* = 8.4 Hz), 6.96 (d, 1H, Ar–H, *J* = 8.2 Hz), 7.04 (d, 2H, Ar–H, *J* = 8.4 Hz), 7.18 (d, 2H, Ar–H, *J* = 8.4 Hz), 7.29 (d, 2H, Ar–H, *J* = 8.4 Hz), 7.53 (d, 2H, Ar–H, *J* = 8.4 Hz), 8.21 (d, 2H, Ar–H, *J* = 8.4 Hz), 8.27 (d, 2H, Ar–H, *J* = 8.4 Hz), 9.46 (s, 1H, OH phenol), 9.70 (s, 1H, OH phenol), 12.10 (s, 1H, NH imidazole ring). ¹³C NMR (100 MHz, DMSO-*d*₆, δ in ppm): 108.07, 110.59, 112.69, 115.65, 116.11, 118.78, 120.11, 124.77, 124.83, 126.66, 127.90, 129.29, 130.20, 130.53, 133.03, 135.96, 142.95, 143.15, 143.79, 147.40, 156.48, 156.90, 158.01, 158.84 and 162.34. Elemental analysis calculated for C₃₃H₂₂N₄O₈: C, 65.78%; H, 3.65%; N, 9.30% and found: C, 65.71%; H, 3.68%; N, 9.29%.

2.3.3. Synthesis of 4,4'-(2-(2,4-bis(4-aminophenoxy)phenyl)-1H-imidazole-4,5-diyl) diphenol (3)

To a 250 mL round-bottomed three-necked flask equipped with a dropping funnel, a reflux condenser and a magnetic stir bar, 6.02 g (0.01 mol) 4,4'-(2-(2,4-bis(4-nitrophenoxy)phenyl)-1H-imidazole-4,5-diyl)diphenol and 0.2 g palladium on activated carbon (Pd/C, 10%), were dispersed in 80 mL ethanol. The suspension solution was heated to reflux, and 8 mL of hydrazine monohydrate was added slowly to the mixture. After a further 5 h of reflux, the solution was filtered hot to remove Pd/C, and the filtrate was cooled to give white crystals. The product was collected by filtration and dried in vacuum oven at 80 °C. The yield of the reaction was 81% (4.4 g), and the melting point was 273–275 °C. FT-IR (KBr disk) at cm^{-1} : 3222–3546 (OH, NH₂ and NH imidazole), 3111 (C–H aromatic), 1615 (C=N), 1588 (C=C), 1258 and 1236 (C–O). ¹H NMR (DMSO-*d*₆, δ in ppm): 5.03 (s, 2H, NH), 5.40 (s, 2H, NH), 6.06 (dd, 1H, Ar–H, *J* = 8.0 Hz), 6.28 (d, 1H, *J* = 2.4 Hz), 6.51 (d, 2H, Ar–H, *J* = 8.4 Hz), 6.58 (dd, 2H, Ar–H, *J* = 8.4 Hz), 6.62 (s, 1H, Ar–H), 6.65–6.69 (m, 4H, Ar–H), 6.76 (dd, 2H, Ar–H, *J* = 8.40), 6.92 (d, 2H, Ar–H, *J* = 8.20), 7.01 (dd, 2H, Ar–H, *J* = 8.40), 7.22 (dd, 2H, Ar–H, *J* = 8.40), 9.43 (s, 1H, OH phenol), 9.61 (s, 1H, OH phenol), 13.92 (s, 1H, NH imidazole ring). ¹³C NMR (100 MHz, DMSO-*d*₆, δ in ppm): 104.15, 106.77, 107.93, 114.40, 115.23, 115.66, 115.74, 120.69, 121.93, 124.70, 124.85, 126.98, 127.65, 129.56, 130.10, 133.10, 133.45, 144.38, 144.86, 146.39, 149.70, 156.77, 157.73, 159.96 and 160.71. Elemental analysis calculated for C₃₃H₂₆N₄O₄: C, 73.06%; H, 4.80%; N, 10.33% and found: C, 73.01%; H, 4.93%; N, 10.29%.

2.4. PAs synthesis

2.4.1. Direct polycondensation using TPP/NMP/Py/LiCl

Into a 50 mL three-necked round-bottomed flask equipped with a condenser, a mechanical stirrer and a nitrogen gas inlet tube, monomer 3 (1 mmol, 0.54 g), a dicarboxylic acid (1 mmol), and LiCl (0.30 g) were dissolved in a mixture of Py (1 mL), TPP (1.20 mmol), and NMP (5 mL). The mixture was heated at 50 °C for 6 h and at 70 °C for 4 h with stirring under dry N₂ atmosphere. The homogeneous solution was poured into a 9 cm diameter glass culture dish, which was heated under vacuum at 80 °C for 1 h, 100 °C for 2 h, and 140 °C for 5 h to evaporate the solvent slowly. Polymer films were self-stripped off from the glass surface by soaking in water. The polymer films were further dried in a vacuum oven at 160 °C for 6 h.

2.4.2. Direct polycondensation using TPP/IL

Into a 50 mL three-necked round-bottomed flask fitted with a water cooled condenser, a mechanical stirrer and a nitrogen gas inlet tube, a mixture of compound 3 (1 mmol, 0.54 g), a dicarboxylic acid (1 mmol), 1,3-dipropyl imidazolium bromide ([1,3-(*pr*)₂im]Br) (0.70 g), and TPP (1.29 mmol) was placed. The mixture was heated at 110 °C for 2.5 h, the solution became viscous as the reaction proceeded. The reaction mixture was then cooled to room temperature and the resulting polymers were precipitated in 100 mL methanol. The precipitate was filtered and washed with hot water, and then was further purified by washing with refluxing methanol for 24 h in a Soxhlet apparatus to remove the low molecular weight oligomers. The inherent viscosity (η_{inh}) of the resulting PAs, measured at a concentration of 0.5 g/dL in NMP at 25 °C, was between 0.52 and 0.91 dL g⁻¹. The above procedure was used for the preparation of all PAs, as shown in Scheme 1.

PA1: Yield = 88% and $\eta_{\text{inh}} = 0.72$ dL/g. FT-IR (KBr disk) at cm^{-1} : 3194–3483 (OH, NH amide and NH imidazole), 3094 (C–H aromatic), 1682 (C=O amide), 1611 (C=N), 1543 (C=C), 1252 and 1214 (C–O). ¹H NMR (DMSO-*d*₆, δ in ppm): 6.20–8.08 (m, 23H, Ar–H), 9.50 (s, 1H, OH phenol), 9.66 (s, 1H, OH phenol), 10.48 (s, 1H, NH amide), 10.59 (s, 1H, NH amide), 13.63 (s, 1H, N–H, imidazole ring). Elemental analysis calculated for (C₄₁H₂₈N₄O₆)_n: C, 73.21%; H, 4.17%; N, 8.33%. Found: C, 73.16%; H, 4.20%; N, 8.33%.

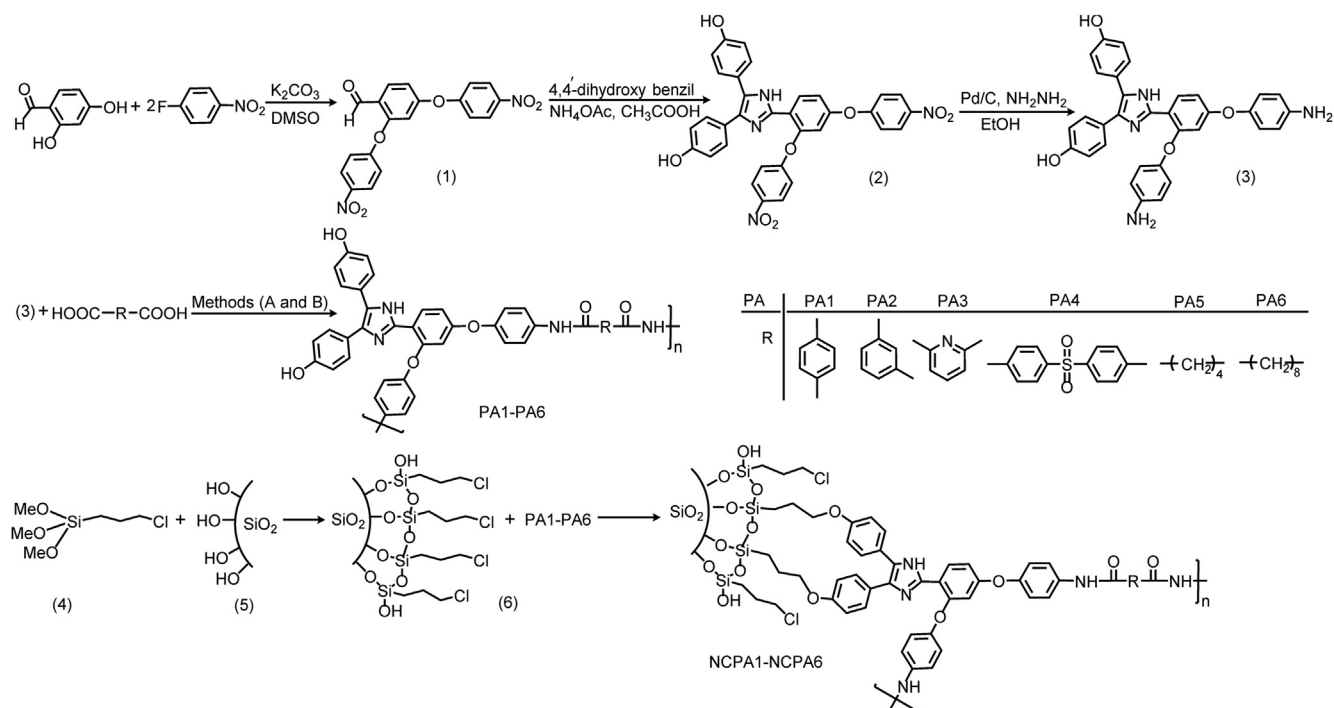
PA2: Yield = 83% and $\eta_{\text{inh}} = 0.67$ dL/g. FT-IR (KBr disk) at cm^{-1} : 3250–3559 (OH, NH amide and NH imidazole), 3039 (C–H aromatic), 1666 (C=O amide), 1610 (C=N), 1522 (C=C), 1256 and 1217 (C–O). ¹H NMR (DMSO-*d*₆, δ in ppm): 6.08–7.99 (m, 23H, Ar–H), 9.44 (s, 1H, OH phenol), 9.65 (s, 1H, OH phenol), 10.43 (s, 1H, NH amide), 10.59 (s, 1H, NH amide), 13.51 (s, 1H, N–H, imidazole ring). Elemental analysis calculated for (C₄₁H₂₈N₄O₆)_n: C, 73.21%; H, 4.17%; N, 8.33%. Found: C, 73.09%; H, 4.29%; N, 8.30%.

PA3: Yield = 89% and $\eta_{\text{inh}} = 0.91$ dL/g. FT-IR (KBr disk) at cm^{-1} : 3272–3538 (OH, NH amide and NH imidazole), 3066 (C–H aromatic), 1671 (C=O amide), 1607 (C=N), 1517 (C=C), 1258 and 1213 (C–O). ¹H NMR (DMSO-*d*₆, δ in ppm): 6.20–8.33 (m, 22H, Ar–H), 9.49 (s, 1H, OH phenol), 9.65 (s, 1H, OH phenol), 10.99 (s, 1H, NH amide), 11.08 (s, 1H, NH amide), 13.52 (s, 1H, N–H, imidazole ring). Elemental analysis calculated for (C₄₀H₂₇N₅O₆)_n: C, 71.32%; H, 4.01%; N, 10.40%. Found: C, 71.16%; H, 4.37%; N, 10.37%.

PA4: Yield = 90% and $\eta_{\text{inh}} = 0.66$ dL/g. FT-IR (KBr disk) at cm^{-1} : 3285–3561 (OH, NH amide and NH imidazole), 3068 (C–H aromatic), 1687 (C=O amide), 1608 (C=N), 1519 (C=C), 1256 and 1219 (C–O). ¹H NMR (DMSO-*d*₆, δ in ppm): 6.43–8.34 (m, 27H, Ar–H), 9.51 (s, 1H, OH phenol), 9.67 (s, 1H, OH phenol), 10.55 (s, 1H, NH amide), 10.59 (s, 1H, NH amide), 13.51 (s, 1H, N–H, imidazole ring). Elemental analysis calculated for (C₄₇H₃₂N₄O₈S)_n: C, 69.46%; H, 3.94%; N, 6.90%. Found: C, 69.37%; H, 4.01%; N, 6.90%.

PA5: Yield = 93% and $\eta_{\text{inh}} = 0.52$ dL/g. FT-IR (KBr disk) at cm^{-1} : 3255–3519 (OH, NH amide and NH imidazole), 3052 (C–H aromatic), 1677 (C=O amide), 1612 (C=N), 1523 (C=C), 1251 and 1206 (C–O). ¹H NMR (DMSO-*d*₆, δ in ppm): 1.63 (m, 4H, C–H), 2.32 (t, 4H, C–H), 6.68–8.25 (m, 19H, Ar–H), 9.40 (s, 1H, OH phenol), 9.55 (s, 1H, OH phenol), 10.53 (s, 1H, NH amide), 10.59 (s, 1H, NH amide), 13.40 (s, 1H, N–H, imidazole ring). Elemental analysis calculated for (C₃₉H₃₂N₄O₆)_n: C, 71.78%; H, 4.91%; N, 8.59%. Found: C, 71.68%; H, 5.04%; N, 8.55%.

PA6: Yield = 96% and $\eta_{\text{inh}} = 0.61$ dL/g. FT-IR (KBr disk) at cm^{-1} : 3258–3526 (OH, NH amide and NH imidazole), 3060 (C–H aromatic), 1668 (C=O amide), 1609 (C=N), 1518 (C=C), 1251 and



Scheme 1. Synthesis of target monomer (3), preparation of polyamides with different dicarboxylic acids (PA1-PA-6) and chemically bonded nanocomposites (NCPA1-NCPA6).

1207 (C–O). 1H NMR (DMSO- d_6 , δ in ppm): 1.30 (m, 8H, C–H), 1.57 (m, 4H, C–H), 2.32 (t, 4H, C–H), 6.64–8.18 (m, 19H, Ar–H), 9.40 (s, 1H, OH phenol), 9.51 (s, 1H, OH phenol), 10.49 (s, 1H, NH amide), 10.52 (s, 1H, NH amide), 13.46 (s, 1H, N–H, imidazole ring). Elemental analysis calculated for $(C_{43}H_{40}N_4O_6)_n$: C, 72.88%; H, 5.65%; N, 7.91%. Found: C, 72.83%; H, 5.70%; N, 7.89%.

2.5. Surface modification of NS particles (mNS)

Silane coupling agent of (3-chloropropyl)trimethoxysilane (CTMS), as shown in Scheme 1, was introduced to ensure good dispersion and improvement of interface between NS particles and PAs. The surface modification of NS particles was carried out as follows [34]. A suspension of 1 g activated NS particles in 30 mL dry toluene was sonicated in 150 W ultrasonic water bath for 1 h, then in a 50 mL round bottomed flask equipped with a reflux condenser, an argon gas inlet tube and a magnetic stir bar, 1 g CTMS in dry toluene (10 mL) was added to this sonicated suspension solution and stirred at 80 °C for 4 h, and then left at room temperature for 24 h. Finally, the separated solid was washed with diethyl ether and then was further purified by washing with refluxing dichloromethane using a soxhlet extraction method and dried under reduced pressure at 60 °C for 12 h. The yield was 1.4 g of covalently anchored CTMS moieties. The modified NS particles (6, Scheme 1) were kept at 60 °C in order to protect the nanoparticles surface from water.

2.6. Preparation of mNS/PA nanocomposites (NCPA)s

0.1 g of one of the PAs was dissolved in 20 mL dry NMP by stirring in an ultrasonic water bath. Then a certain amount of mNS particles (5, 10, 15 and 20 wt% based on weight of PA) was added to the resulting solution and the mixture stirred further for 30 min at 70 °C. After irradiation, 0.2 g K_2CO_3 was added and the mixture was continuously stirred at 80 °C for 5 h under argon atmosphere. At the end of the reaction, the mixture was allowed to cool and after filtration the solid was further purified by washing with refluxing

ethanol using a soxhlet extraction method to remove any unreacted materials. The obtained nanocomposites dried under reduced pressure at 60 °C for 12 h.

A certain amount (5, 10, 15 and 20 wt%) of NCPAs in DMF was stirred in an ultrasonic water bath for 1 h to form a homogeneous dispersion. The mixture was further stirred for 24 h at 60 °C, forming a viscose solution which was casted into flat-bottom glass plate. The casted nanocomposite was heated under nitrogen atmosphere at different temperatures of 70 °C, 100 °C, 200 °C for 1 h each and at 250 °C for 2 h, forming film of NCPAs with thicknesses of around 3 mm.

3. Results and discussion

3.1. Synthesis and characterization of diamine-bisphenol (3)

This manuscript reports selective polycondensation of a new diamine-bisphenol monomer with several commercial aliphatic and aromatic dicarboxylic acids in imidazolium-based ILs. For this purpose, compound 3 containing diamine and dihydroxyl groups were synthesized in three steps. As illustrated in Scheme 1, compound 1 was successfully synthesized from 1-fluoro-4-nitrobenzene and 2,4-dihydroxy benzaldehyde as starting materials by the nucleophilic fluorodisplacement reaction. Compound 1 reacted with 4,4'-dihydroxy benzil and ammonium acetate in a well-known classical but convenient synthetic method for the formation of imidazole ring. The target monomer, compound 3, was obtained by catalytic reduction of the nitro groups of compound 2 by using hydrazine hydrate and Pd/C in refluxing ethanol. The structure of these compounds was identified by elemental analysis, FT-IR and 1H NMR spectroscopy. FT-IR spectrum of compound 1 in Fig. 1 shows the absorption bands of nitro group at 1522 and 1350 cm^{-1} and carbonyl of aldehyde group at 1681 cm^{-1} . 1H NMR spectrum of compound 1 showed proton of aldehyde group at 10.160 ppm. After reaction, the disappearance of absorption band at 1681 cm^{-1} and signal at 10.16 ppm confirmed the consumption of aldehyde group. New signals were observed at 13.91 ppm and at

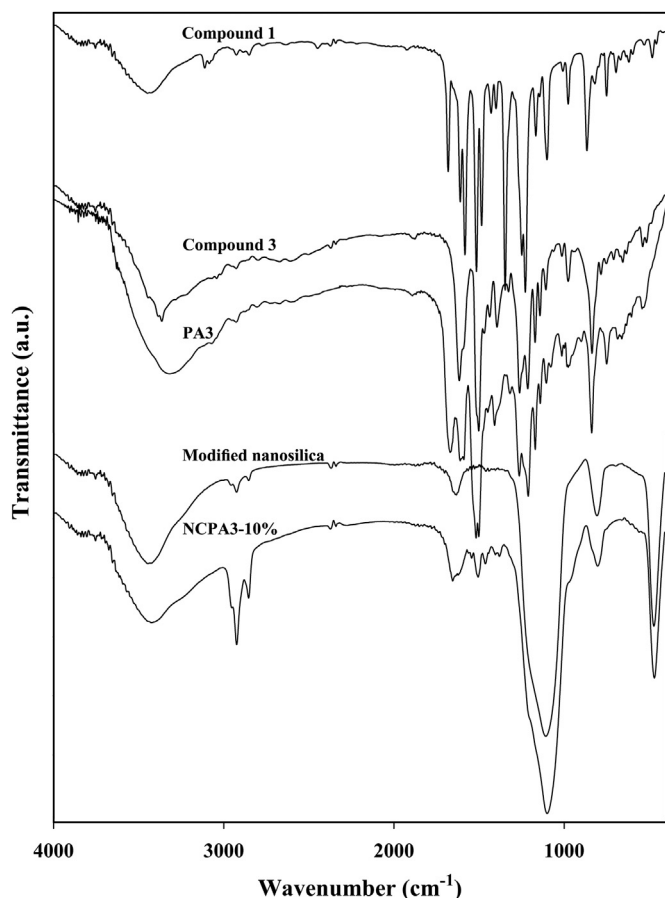


Fig. 1. FT-IR spectra of compounds 1 and 3, PA3, mNS and NCPA3-10%.

9.43–9.60 ppm in the spectrum of compound 3, as shown in Fig. 2, which are related to N–H of imidazole ring and O–H of hydroxyl groups, respectively. After reduction of nitro groups of compound 2, the two characteristic absorption bands at 1521 and 1352 cm^{-1}

(NO_2 asymmetric and symmetric stretchings, respectively) disappeared and the absorption bands of primary amino groups of compound 3, as shown in Fig. 1, were observed at 3473 cm^{-1} and 3386 cm^{-1} with the bending vibrations in the region of 1560–1640 cm^{-1} . As shown in Fig. 2, ^1H NMR spectrum of compound 3 showed the characteristic resonance of different protons of two amine groups at 5.03 and 5.40 ppm and two hydroxyl groups at 9.43 and 9.60 ppm. ^{13}C NMR spectrum of compound 3 showed 25 different carbons for the aromatic and heterocyclic rings.

3.2. Synthesis and characterization of PAs and nanocomposites

As an extension of studies in developing organosoluble high-performance polymers, a simple and efficient method is reported for the selective polymerization of a new diamine-bisphenol monomer with commercial dicarboxylic acids in ILs as activator and solvent. The polycondensation reaction proceeded selectively and efficiently in the mixture of ILs/TPP without using NMP/Py/LiCl mixture which is required when using traditional method by Yamazaki [35]. The ambient temperature ILs, especially those based on 1,3-dialkylimidazolium cations, have gained considerable interest as promising alternative green solvents in polymer synthesis [4,36–38]. This investigation also used room temperature ILs, thermally stable near the process temperature and good solvents for the initial materials and for the resulting polymer, which were prepared simply from the commercially available starting materials such as *N*-trimethylsilylimidazole and alkyl halides [33]. Thus, different symmetrical 1,3-dialkylimidazolium ILs bearing Br, PF_4^- and BF_6^- anions, shown in Table 1, were prepared and used as polycondensation agents. These ILs were all very viscous liquids at room temperature and soluble in polar solvents such as water and methanol allowing for the complete isolation of the obtained polymers. To determine the effect of the nature of ILs on the yield and viscosity of the polymer, the synthesis of aromatic PA3 was carried out in different ILs at a constant reaction temperature of 110 °C. Table 1 compares the yield and viscosity of PA3 in different ILs. Although PA3 was soluble in all ILs, the viscosity of the polymer decreased when the alkyl chain length in the IL increased. This may be explained by the decrease in the polarity of the IL, resulting in a

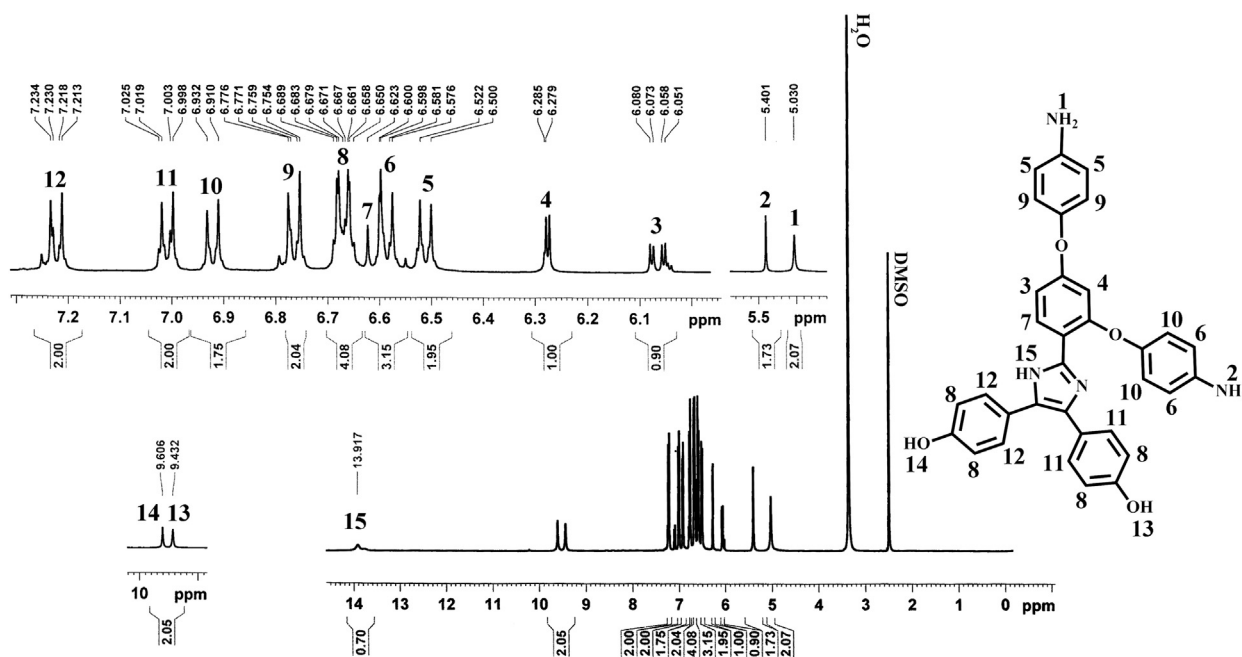


Fig. 2. ^1H NMR spectrum of monomer (3) in DMSO-d_6 .

Table 1
The influence of IL cation and anion upon yield and inherent viscosity (η_{inh}) of PA3.

Polymer	IL structure	IL	Yield (%)	η_{inh}^a
PA3		[1,3-Isopropyl ₂ im]Br	80	0.76
PA3		[1,3-Propyl ₂ im]Br	89	0.91
PA3		[1,3-Butyl ₂ im]Br	77	0.86
PA3		[1,3-Pentyl ₂ im]Br	75	0.67
PA3		[1,3-Hexyl ₂ im]Br	83	0.66
PA3		[1,3-Heptyl ₂ im]Br	89	0.63
PA3		[1,3-Butyl ₂ im]BF ₄	67	0.63
PA3		[1,3-Butyl ₂ im]PF ₆	66	0.61

^a Measured at a concentration of 0.5 g/dL in NMP at 25 °C.

decreased solubility of polymer. The highest viscosity of PA3 was obtained when [1,3-(Pr)₂im]⁺ Br was used as the reaction medium, and this IL was also selected for the synthesis of other PAs. The optimum polycondensation time (2.5 h) was determined by measuring the yield and viscosity of PA3 in the selected IL and at the selected temperature (110 °C). These results are shown in Fig. 3, and the synthetic procedure and polymers designation are shown in Scheme 1. The decrease in viscosity of PA3, as shown in Fig. 3, can be as a result of thermal degradation of the polymer chains at 110 °C in longer reaction times.

A dark colour and insoluble material (PA1'') was obtained when direct polycondensation of compound 3 with terephthalic acid was conducted in the mixture of TPP/NMP/Py/LiCl. This thermoset material (PA1'') has been formed through cross-linking reactions between carboxylic acid groups of terephthalic acid and amino and hydroxyl groups of compound 3. This demonstrates the beneficial effect of ILs in the synthesis of thermoplastic PAs selectively from a diamine-bisphenol compound, in addition to other useful factors

Table 2
Average molecular weights, viscosity and solubility of PAs and nanocomposites.

Code	η_{inh} (dL/g) ^a	M_n (g/mol)	M_w (g/mol)	Moisture absorption (%)	DMSO	DMAc	DMF	NMP	Py	THF	CH ₃ CN	<i>m</i> -cresol
PA1	0.72	32,219	56,920	13.51	++	++	++	++	+	±	–	+
PA2	0.67	30,081	54,223	12.88	++	++	++	++	+	±	–	+
PA3	0.91	36,357	61,368	14.61	++	++	++	++	+	±	–	+
PA4	0.66	29,301	53,984	12.47	++	++	++	++	+	±	–	+
PA5	0.52	26,811	49,124	11.34	++	++	++	++	++	+	–	++
PA6	0.61	22,051	44,755	12.11	++	++	++	++	++	+	–	++
NCPA1-5%	–	–	–	–	–	–	–	–	–	–	–	–
NCPA6-5%	–	–	–	–	±	±	±	±	–	–	–	–
NCPA6-10%	–	–	–	–	–	–	–	–	–	–	–	–
PA1''	–	–	–	–	–	–	–	–	–	–	–	–

GPC measurement at 30 °C with DMF as fluent at 1 mL/min and monodisperse polystyrene as standard for instrumental calibration.

PA1'': This PA was prepared in the mixture of TPP/NMP/Py/LiCl.

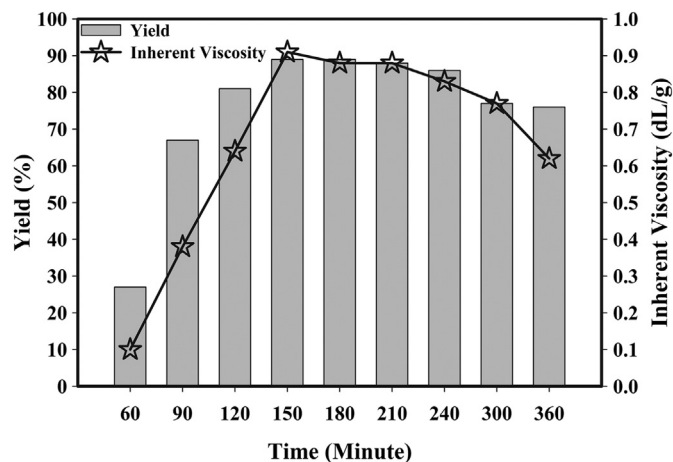


Fig. 3. Optimum conditions for the synthesis of PA3 in IL.

such as the non-volatility of ILs, low reaction time, no environmental pollution, and no need to remove chemicals such as NMP, LiCl and Py which are essential for conventional direct polycondensation. The reason for the selective polycondensation of diamine-bisphenol (compound 3) can be suggested to be due to formation of phenolic salt as a result of reaction between phenolic hydroxyl groups and the ionic liquid, while the amine groups remain free to react with the carboxylic acids to give polyamide. The PAs obtained in IL/TPP mixture were brown powder with good yields (80–96%) after removal of low molecular weight fractions by using hot methanol extraction. Inherent viscosities of these PAs in NMP (0.5 g/dL) were in the range of 0.52–0.91 dL/g. The elemental analysis results were in good agreement with the calculated percentages for carbon, hydrogen and nitrogen contents in PAs repeating units. The weight average molecular weights (M_w) of these PAs were in the range of 44755–61368 g/mol with distribution index of 1.69–2.03. The results are listed in Table 2. ILs possess low vapour pressure and, in contrast to volatile organic solvents, can be used at high temperature and under vacuum. Thus, the relatively high molecular weights of these polymers can be due to the fact that ILs can dilute highly viscous polymer solutions and facilitate the elimination of the byproduct under N₂ flow, thus shifting the equilibrium. The ¹H NMR spectrum of PA3, Fig. 4, shows the N–H proton of amide groups at 10.99–11.08 ppm, N–H proton of imidazole ring at 13.52 ppm and phenolic hydroxyl groups at 9.48–9.65 ppm. The signals of aromatic and aliphatic protons appeared in the range of 6.58–8.88 ppm and 1.25–2.25 ppm, respectively.

PA/mNS composites with covalent bonds between organic and inorganic phases have been successfully prepared. NS were first activated in methanesulfonic acid media for 12 h, and then CTMS

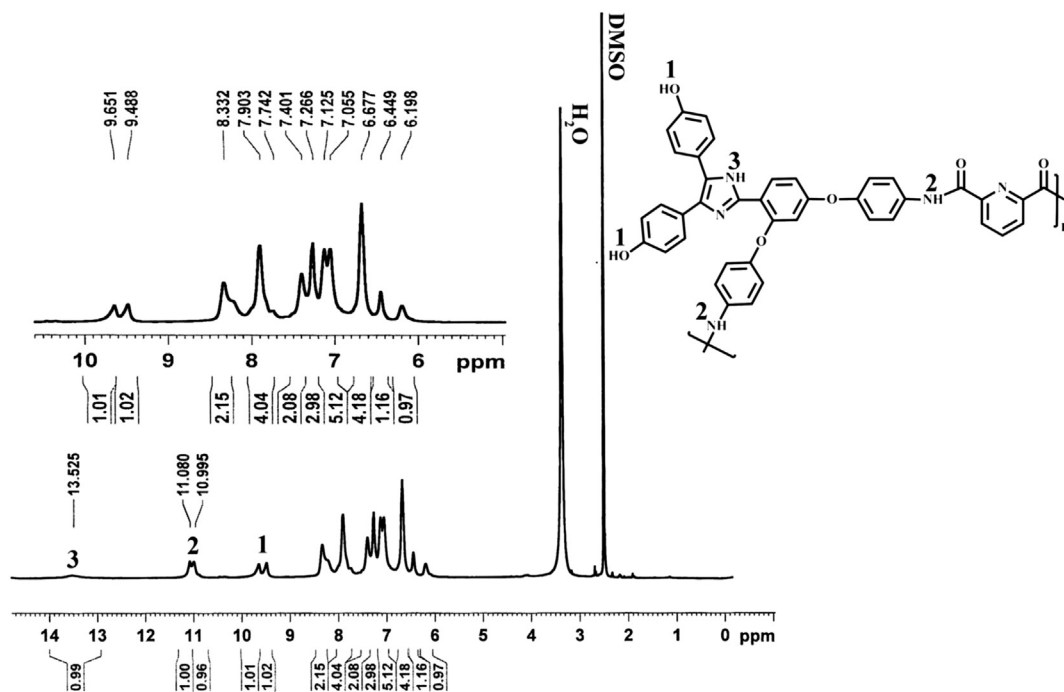


Fig. 4. ^1H NMR spectrum of PA3 in DMSO-d_6 .

molecules were linked to the silica surface via Si–O–Si covalent bonds. This was achieved by condensation of hydroxyl groups (–OH) on the surface of activated silica with the hydrolysable methoxy groups (– OCH_3) of CTMS. FT-IR spectrum of mNS in Fig. 1 presents a few absorption bands; around 1100 cm^{-1} can be assigned to the characteristic vibration bands of Si–O link, at 3400 cm^{-1} to the characteristic stretching vibration of hydroxyl group (–OH) on the surface of NS, at 1380 cm^{-1} to the bending and at $2906\text{--}2857\text{ cm}^{-1}$ to the stretching vibrations of C–H of organic methylene. In addition, characteristic absorption band at $1040\text{--}1180\text{ cm}^{-1}$ broadens which reveals that a new absorption band of Si–O–Si has formed due to the contribution of interaction between siloxane and NS. The above interpretations, and also the insolubility of the nanocomposites in organic solvents (Table 2), are enough to suggest that CTMS is chemically bound on the surface of NS. PA/mNS composite was prepared from chloro-displacement reaction of mNS with the hydroxyl groups of PAs. FT-IR spectrum of NCPA3–10% nanocomposite, Fig. 1, exhibited the characteristic absorption bands of the amide group in the regions of 3407 cm^{-1} (N–H stretching) and 1671 cm^{-1} (C=O stretching), and Si–O–Si band at $1040\text{--}1150\text{ cm}^{-1}$. As shown in Scheme 1, it is suggested that covalent bonds can be formed between polymer matrix and mNS through substitution reaction of phenolic groups in the polymer backbones with the chlorine atom on the surface of mNS. It was not possible to obtain ^1H NMR spectrum from composite samples due to their insolubility in organic solvents. X-ray scattering is well-suited for many polymer/inorganic composites. X-ray diffraction (XRD) technique has been used to investigate the nature of the nanocomposites with respect to pure PAs. XRD patterns for pure PA1, NS, mNS and nanocomposites (NCPA1–5% and NCPA1–15%) are shown in Fig. 5. According to the XRD patterns for pure PAs and NS, they are considered totally amorphous in nature which do not show any sharp diffraction peaks. XRD patterns of mNS and nanocomposites containing 5% and 15% mNS (NCPA1–5% and NCPA1–15%) showed sharp diffraction peaks which might be related to small structural order in the mNS, Scheme 1 (6). The number of these sharp peaks increased with increasing mNS content in the

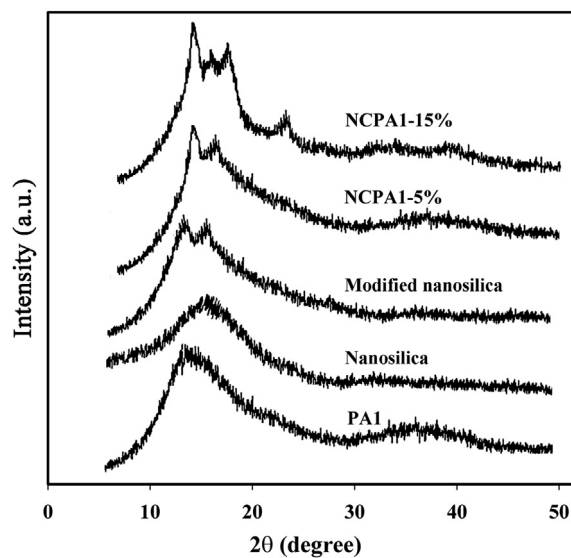


Fig. 5. X-ray diffraction patterns of PA (1, 3, and 5), NS, mNS, NCPA1–(5% and 15%).

polymer matrix. To study the electrochemical behaviour of PAs and nanocomposites, modified graphite-polymer paste as working electrode was examined by cyclic voltammetry (CV) and the results in Fig. 6 reveal that the polymers are oxidized at a potential of $0.5\text{--}0.8\text{ V}$. The two anodic peaks at the forward scan of potential, at 0.6 and 0.8 V , may be related to the oxidation of the –OH groups and imidazole ring, respectively. The CV curves show that PA1 has higher electrochemical oxidation potential in comparison with the nanocomposites. The intensity of oxidation peak of –OH groups in the polymer backbone in the region of 0.6 V decreased with increasing the amount of mNS from 5 wt% to 20 wt%. Therefore, it can be concluded that the –OH groups in the polymer backbone are the main sites for chemical bond formation with mNS, and also for electrochemical oxidation to occur. The oxidized products are

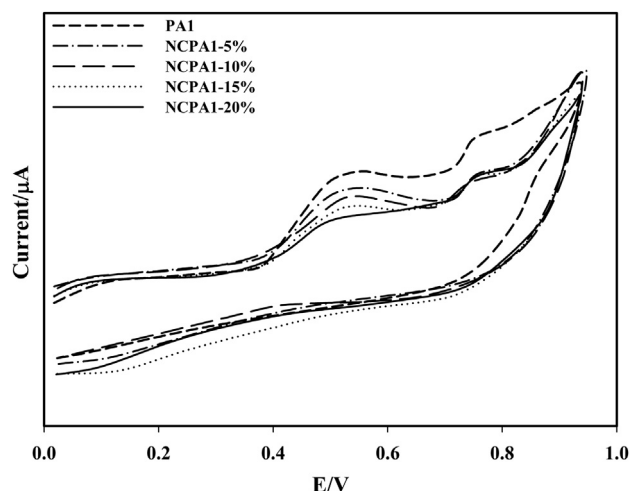


Fig. 6. Cyclic voltammograms of PA1 and NCPA1-5%–20% with modified CPE.

formed irreversibly during forward scan and there is not cathodic peak at the backward scan.

3.3. Properties of PAs and nanocomposites

3.3.1. Solubility and moisture absorption

As a general rule, high solubility is a desired prerequisite for polymer processing. The solubility behaviour of these PAs and nanocomposites was qualitatively tested in various organic solvents, and the results are summarized in Table 2. All PAs prepared in the mixture of TPP/IL exhibited excellent solubility in polar aprotic solvents such as NMP, DMAc, DMF, DMSO and even in less polar solvents like pyridine, THF, and *m*-cresol, while PA1' which was prepared in the mixture of TPP/NMP/Py/LiCl did not dissolve in the above mentioned solvents. In previous reports, comparable aramids with almost the same backbone structure, showed very low solubility in organic solvents [39] or were practically insoluble [40]. The good solubility should be due to presence of different functional groups in the polymer backbone such as bulky heterocyclic pendant, ether linkage, hydroxyl groups, and unsymmetrical structure. These factors and also the amorphous nature contributed to the enhanced solubility of these PAs through better penetration of solvent molecules, formation of H-bonding and dipole–dipole interaction with polar molecules of organic solvents. In addition, the solubility varies depending upon the dicarboxylic acid used. The PAs which were synthesized from aliphatic dicarboxylic acids (PA5 and PA6) exhibited better solubility behaviour in less polar solvents such as THF and *m*-cresol. The presence of methylene units instead of rigid phenyl improves the solubility of these PAs. Composites of aliphatic PA6 with 5 wt% mNS showed partial solubility in highly polar solvents by heating at 60 °C which can be due to solution of low molecular weight oligomer component. However, composites containing more than 5 wt% mNS did not dissolve in these solvents which confirm they have definitely formed cross-linked network structure through chemical reaction between CH_2Cl groups in the mNS and hydroxyl groups in the polymer backbone. The water uptake determines the final application of high performance materials. The absorbed water diminish T_g and influence mechanical and electrical properties, but in membrane technology, greater water uptake implied better performance. The results showed moisture intake of these PAs ranged from 11.34% to 14.61%, as listed in Table 2. These PAs are partially hydrophilic materials because of the presence of bulky pendant which increase the free volume and their polar amide and free hydroxyl groups which interact effectively with water molecules.

3.4. Photophysical properties

The photophysical properties of PAs and nanocomposites were investigated by using UV–vis and fluorescence spectroscopy. The absorption and fluorescence spectra of PAs and nanocomposites films are shown in Fig. 7. The absorption spectra of PAs in dilute NMP solution (0.2 g/dL) and in films, Fig. 7A, were nearly identical and the maximum absorption wavelengths (λ_{ab}) were in the range of $\lambda_{ab} = 302\text{--}317$ nm, as listed in Table 3, which shows a relatively small energy band gap for $\pi \rightarrow \pi^*$ transition. Reasonably, this could be attributed to the all aromatic structure possessing substituted imidazole pendant attached to the aromatic backbone. To investigate the fluorescence emission of PAs, an excitation wavelength of 320 nm was used in all cases. The fluorescence emission spectra of PAs are shown in Fig. 7B. The solution and thin films of PAs showed broad fluorescent emission spectra with the maximum wavelengths in the range of $\lambda_{em} = 421\text{--}499$ nm and $\Phi_f = 12\text{--}38\%$, as listed in Table 3. The aliphatic PAs (PA5 and PA6) exhibited blue emission ($\lambda_{em} = 421\text{--}445$ nm) with the highest Φ_f values of 31% and 38%, respectively. The aromatic PAs exhibited green emission ($\lambda_{em} = 480\text{--}490$ nm) and Φ_f in the range of 12–17%. The blue shift and higher intensity of PL of semi-aromatic PAs compared with the PL of aromatic PAs could be attributed to the effectively reduced conjugation and capability of charge transfer complex formation by aliphatic diacids in comparison with the electron-donating amino unit and the strongly electron-accepting aromatic diacid unit [41]. The absorption and emission spectra of the representative nanocomposite films are shown in Fig. 7(A and B). Table 3 lists some important photophysical data obtained from films and suspension solution of composites containing 5 wt% mNS. The nanocomposites showed absorption at $\lambda_{ab} = 315\text{--}329$ nm, emission at $\lambda_{em} = 441\text{--}503$ nm and $\Phi_f = 22\text{--}41\%$. As can be seen in Fig. 7B and in Table 3, similar to aliphatic PAs their nanocomposites (NCPA5-5% and NCPA6-5%) also showed blue shift with Φ_f of 39% and 41%, respectively, in comparison with the nanocomposites of aromatic PAs which showed green shift with $\Phi_f = 16\text{--}22\%$.

3.5. Mechanical properties

The tensile stress–strain curve is a tool to provide data on toughness (area under the curve), ultimate tensile strength, ultimate elongation at break and Young's modulus. Typical stress–strain curves of PAs and the nanocomposites are illustrated in Fig. 8 and the corresponding tensile data are summarized in Table 4. An average of five individual measurements was used for each sample. These PAs showed tensile strength in the range of 48–88 MPa, elongation to break of 14–26%, and initial modulus of 1.61–2.47 GPa. The PA1' which was prepared in the mixture of TPP/Py/NMP/LiCl, as explained in section 3.2, is a highly crosslinked material and showed very brittle characteristics with low elongation (0.6%) and high Young's modulus (6.0 GPa), as listed in Table 4. The area under the stress–strain curve is used to measure the fracture energy or static toughness of the polymer and depends on the molecular weight and intermolecular interactions. PA1 showed the highest tensile strength and toughness due to higher molecular weight and more symmetrical structure of terephthalic unit in comparison with the other PAs. PA5 and PA6 showed the lowest strength and elongation due to presence of aliphatic chain in the backbone and lower molecular weights in comparison with the other PAs. From Table 4, we can see the noticeable trend of tensile strength of specimens increased when increasing the mNS amount. The tensile strength of PA1 increased from 88 MPa to 110 MPa for NCPA1-20%, and simultaneously, the tensile elongation decreased from 26% to 9%. The enhancement of tensile strength corresponds to the forecast, as mentioned before, that NS could play a

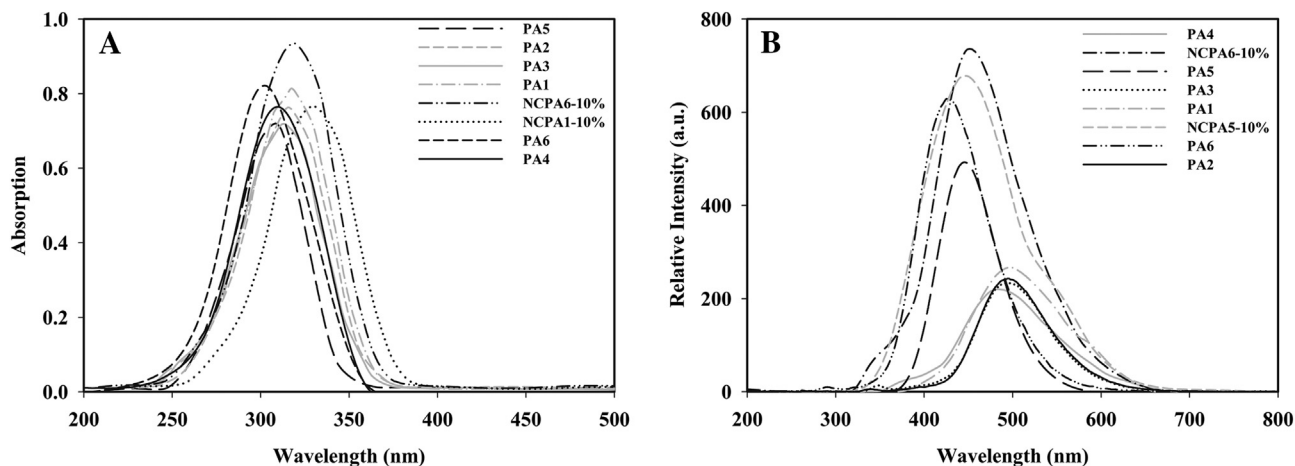


Fig. 7. UV-vis and fluorescence spectra of PAs, NCPA1-10% and NCPA6-10%.

Table 3
Optical properties data of PAs and nanocomposite.

Code	λ_{ab} (nm) ^a	λ_{em} (nm) ^a	λ_{ab} (nm) ^b	λ_{em} (nm) ^b	Φ_f^c (%)
PA1	314.75	498.00	317.00	499.00	17
PA2	313.25	495.25	315.75	497.25	15
PA3	311.50	496.25	315.00	497.25	14
PA4	310.25	480.25	311.50	483.75	12
PA5	307.50	442.75	308.25	445.25	31
PA6	302.50	421.00	302.25	423.25	38
NCPA1-5%	321.25	502.50	329.50	502.75	22
NCPA2-5%	320.00	499.25	326.25	500.25	20
NCPA3-5%	318.25	496.25	324.25	499.00	17
NCPA4-5%	317.25	487.00	321.25	488.00	16
NCPA5-5%	315.00	454.00	320.25	453.75	39
NCPA6-5%	315.50	440.75	317.50	443.50	41
NCPA6-10%	–	–	318.75	449.25	–
NCPA6-15%	–	–	320.75	451.25	–
NCPA6-20%	–	–	321.50	452.25	–

Polymer concentration of 0.20 g/dL in NMP.

^a UV-visible absorption and fluorescence emission spectra of the PAs and nanocomposites (5% NS) in solution.

^b UV-visible absorption and fluorescence emission spectra of the PAs and nanocomposites (5% NS) in films

^c Fluorescence quantum yield relative to 10^{-5} M quinine sulphate in 1 N H_2SO_4 (aq) ($\Phi_f = 0.55$) as a standard.

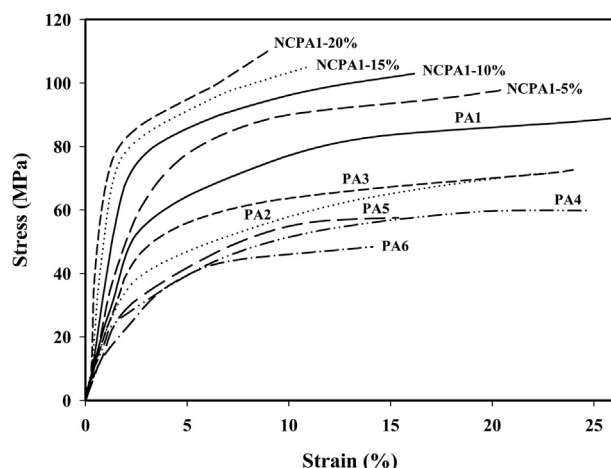


Fig. 8. Tensile stress vs. strain (%) of PAs and NCPAs nanocomposites.

reinforcing role in the composite. It might be ascribed to the presence of chemical interactions between mNS and hydroxyl groups in the PAs chains and formation of cross-links. As we know, elongation at break is a crucial parameter to judge the plasticity or ductility of the polymer. Generally, the addition of inorganic particles into polymers, and in this case formation of cross-links, lowers the elongation at break.

3.6. Thermal properties

The thermal behaviour data of these PAs and nanocomposites were assessed by using DSC, DMTA and TGA analysis. Fig. 9 shows DSC curves of PAs, neither crystallization exotherms nor melting endotherms were observed in the range of 35–400 °C, so that these PAs were considered to be essentially amorphous. The amorphous nature of these PAs can be attributed to their bulky pendant group which decreased the inter-chain interaction resulting in loose polymer chain packaging and aggregates. The T_g values were read at the middle of the first break down observed in the DSC curves, and found to be in the range of 188–325 °C, as listed in Table 4. In general, molecular packing and chain rigidity are among the main factors influencing on T_g values. Therefore, the increased rotational barrier caused by the bulky pendant in the monomer 3 and side chain-side chain and side chain-main chain interactions enhanced T_g values. As anticipated, the T_g values of these PAs also depend on the stiffness of dicarboxylic acid component in the polymer chain and the increasing order of T_g generally correlated with that of chain rigidity. PA5 and PA6 obtained from aliphatic dicarboxylic acid, showed lower T_g values (204 °C and 188 °C, respectively) because of the presence of flexible aliphatic unit and their low rotation barrier, and the highest T_g value of 325 °C was observed for PA1 derived from terephthalic acid. T_g values of composites showed dependence on the amount of mNS particles. As shown in Table 4, composites of aromatic PAs containing more than 5 wt% mNS did not show T_g up to 400 °C, while T_g of PA1 increased from 325 °C to 344 °C when contains 5 wt% mNS.

The viscoelastic behaviour of representative PAs and nanocomposites was determined by using DMTA. $\tan \delta$ curves are shown in Fig. 10A. Measurement of $\tan \delta$ values was carried out to relate the viscoelastic behaviour and PAs molecular structure and mNS content in the composites. The increase in the T_g (peak temperatures in the $\tan \delta$ curves) values indicates that a change in the viscoelastic behaviour of the nanocomposite films from liquid like to solid-like occurs. As already has been discussed, mNS particles and PA chains have definitely been involved in reactions of cross-

Table 4
Thermal and mechanical properties of PAs and nanocomposites.

Code	Tensile (MPa) ^a	Modulus (GPa)	Elongation (%)	T _g (°C) ^b	T ₁₀ (°C) ^c	T ₁₀ (°C) ^c	C. Y. ^d	C. Y. ^d	LOI (%) ^e
PA1	88.41	2.47	25.82	325.36	511.25	455.81	63.11	–	42.74
PA1'	117.19	6.00	0.90	–	532.49	489.26	70.65	–	45.76
PA2	71.08	2.10	22.73	304.42	498.08	450.19	58.49	–	40.90
PA3	71.67	2.18	23.58	260.17	471.91	430.04	51.05	–	37.92
PA4	59.38	1.94	24.17	310.64	501.47	451.70	58.68	–	40.97
PA5	56.85	1.78	15.28	203.76	462.60	416.67	40.91	–	33.86
PA6	47.72	1.61	14.14	188.24	447.15	407.33	41.28	–	34.01
NCPA1-5%	97.54	2.51	20.21	344.39	528.24	475.51	72.40	10.24	46.46
NCPA1-10%	101.63	2.67	16.06	–	533.58	488.58	73.39	15.08	46.86
NCPA1-15%	104.90	2.92	10.80	–	539.03	495.04	75.00	17.63	47.50
NCPA1-20%	110.76	3.12	8.73	–	538.79	506.43	75.18	24.00	47.57
NCPA2-10%	–	–	–	–	530.65	482.72	69.45	16.49	45.28
NCPA3-10%	–	–	–	–	525.84	471.75	62.24	12.53	42.40
NCPA4-10%	–	–	–	–	530.03	484.34	71.39	17.44	46.06
NCPA5-10%	–	–	–	231.85	517.43	434.18	51.55	–	38.12
NCPA6-10%	–	–	–	206.06	460.71	423.00	50.14	–	37.56

PA1': This PA was prepared in the mixture of TPP/NMP/Py/LiCl.

^a Film stored in a 80% relative humidity atmosphere before tensile test.

^b T_g was recorded by DSC at 10 °C/min in N₂.

^c T_{10%} was recorded by TGA at 10 °C/min in N₂ and in air, respectively.

^d C.Y. = Char yield, weight% of material left at 800 °C in N₂ and in air, respectively.

^e Limiting oxygen index percent evaluating at char yield 800 °C.

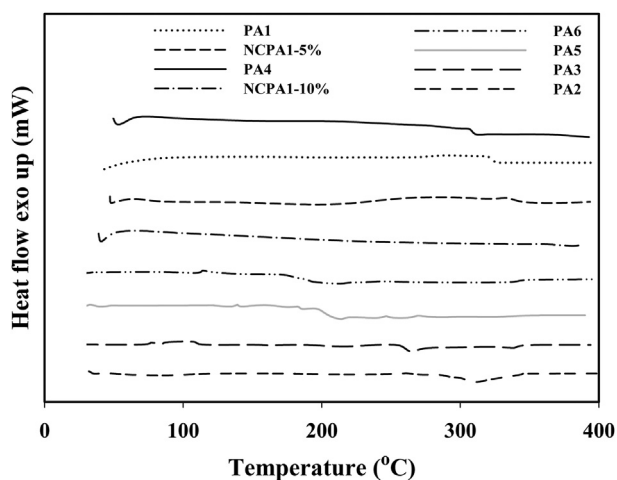


Fig. 9. DSC curves of PAs and NCPA1-5% and NCPA1-10% under N₂ at 10 °C/min.

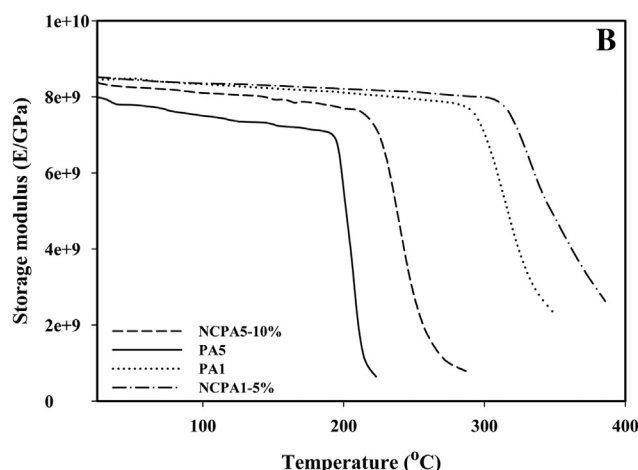
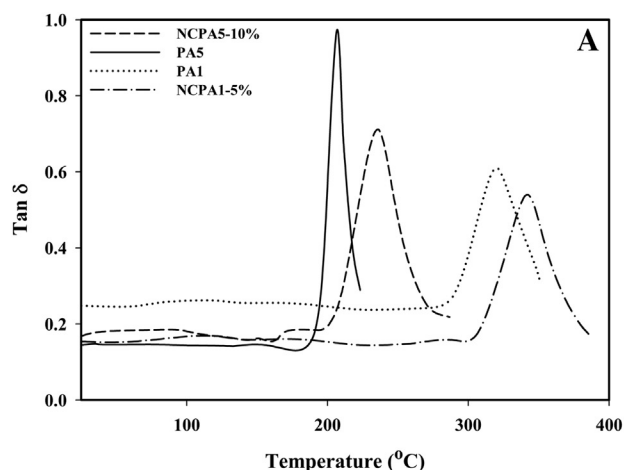


Fig. 10. DMTA curves of tan δ (A) and storage modulus (B) of PA (1, 5) and NCPA1-(5% and 10%).

links formation. These immobilize the polymer chains at elevated temperatures. The T_g values of the representative PAs (PA1 and PA5) were in the range of 205 °C and 320 °C, respectively, and also for the nanocomposites (NCPA5-10% and NCPA1-5%) were 235 °C and 340 °C. These values were in good agreement with T_g values of these polymers measured by DSC method. Thermoplastic response of PAs and their nanocomposites was determined by plotting storage modulus against testing temperature. Fig. 10B shows the storage modulus values as a function of varying wt% of mNS particles. It was observed that with increasing wt% of mNS particles the value of storage modulus of composite increases.

Fig. 11A presents TGA curves of the PAs, and the corresponding 10% weight loss temperatures (T_{10%}) determined from the original curves in N₂ (447–511 °C) and air (407–456 °C) are listed in Table 4. Char yield (CR) can be used as criteria for evaluating limiting oxygen index (LOI) of the polymers in accordance with Van Krevelen and Hoftyzer equation [42], LOI = 17.5 + 0.4CR. In general, when the LOI of a polymer is higher than 26% it is considered to be flammable. For these PAs, LOI values were calculated based on their char yields at 650 °C. According to Table 4, thermal stability of the aromatic PAs in N₂ appeared in the 472–511 °C range in terms of T_{10%} values, compared to 447–463 °C for the aliphatic PAs. This can

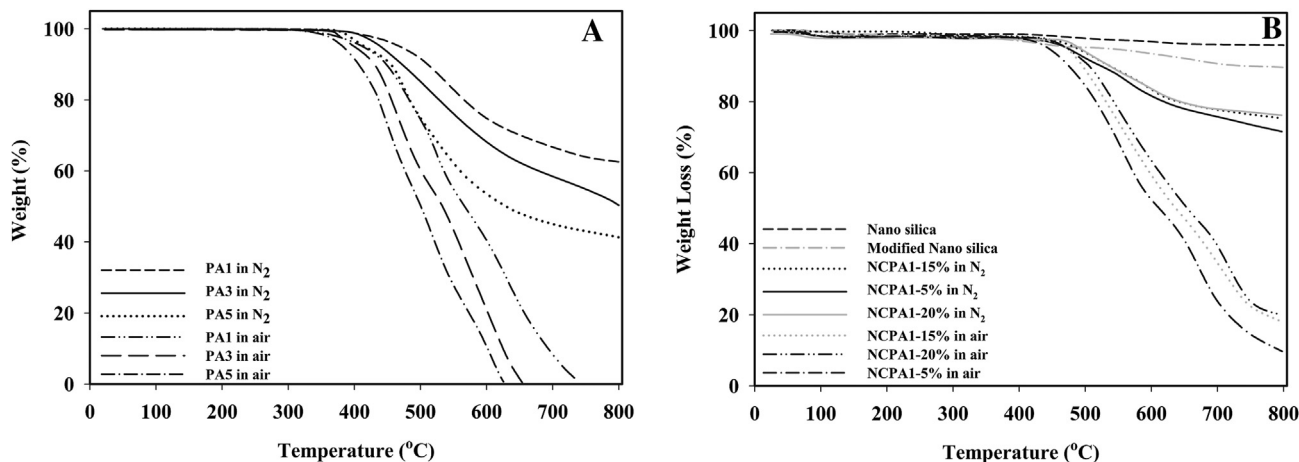


Fig. 11. TGA curves of (A) PA (1, 3 and 5), and (B) NS, mNS, NCPA1-(5%, 15% and 20%) under N₂ and air at 10 °C/min.

be pertained to the rigid structure of aromatic diacids compared to the flexible structure of aliphatic diacids. Fig. 11B shows TGA curves of NS, mNS and composites containing 5, 15 and 20 wt% mNS particles, and the thermal data extracted from the original curves are listed in Table 4. The $T_{10\%}$ value of NCPA1-20% in comparison with the same pure PA1 has increased from 511 °C to 539 °C with the char yield from 63% to 76% in N₂. It is clear that the existence of inorganic material in polymer matrix and its chemical interactions

with the polymer shifted decomposition temperature towards higher temperatures indicating enhanced thermal stability of the composite with mNS loading.

3.7. Extraction of metal cations from aqueous solution

Heavy metals are toxic because they are present as ions in an aqueous system and can be readily absorbed into the human body.

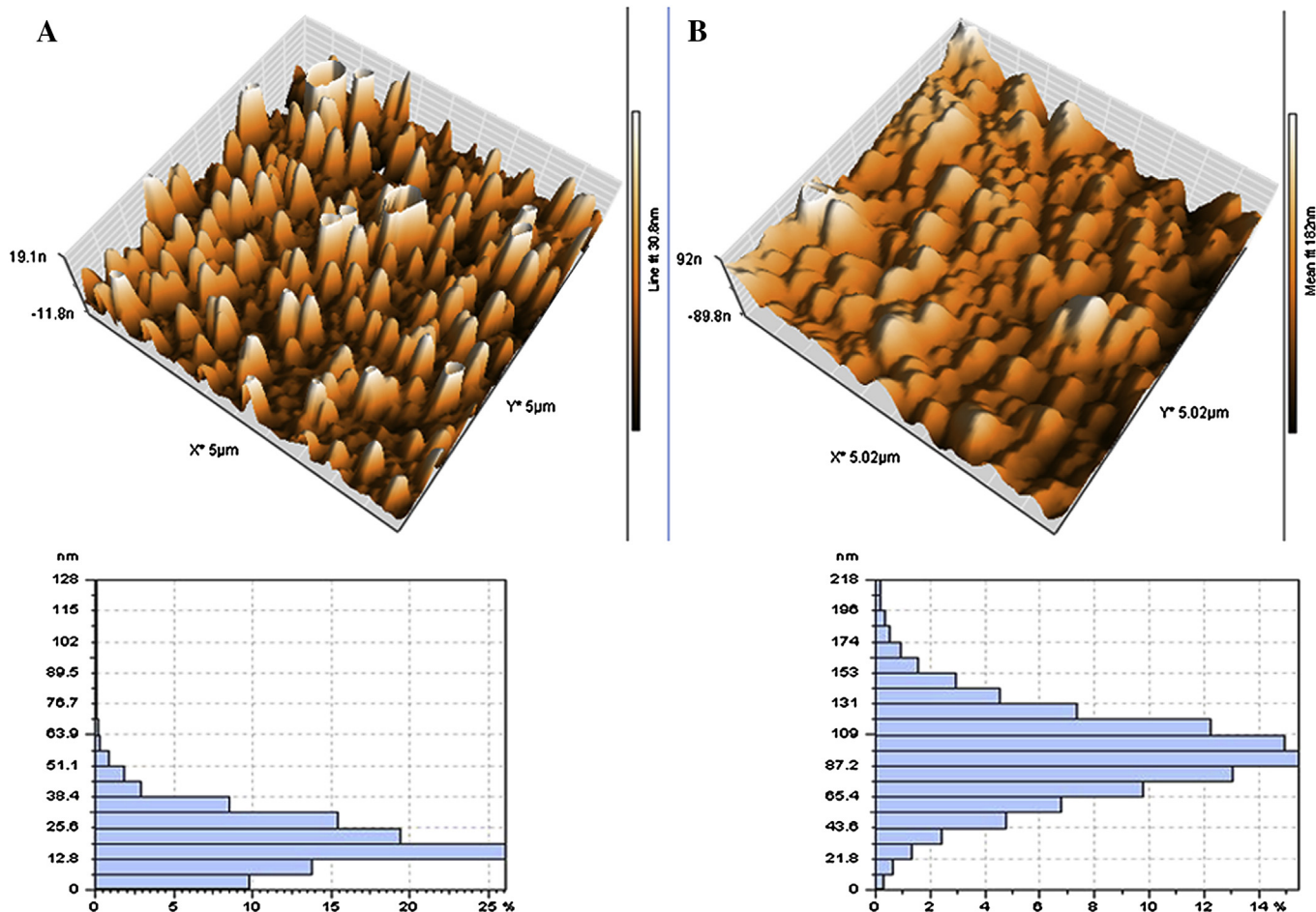


Fig. 12. AFM images of NCPA1-10% (A) before and (B) after absorption of Hg^{II}.

Thus, the removal of metal ions from water has become an important and widely studied area. In these experiments, the presence of imidazole rings, amide linkages and hydroxyl groups in the backbones of solid PAs can act as hosts for the adsorption and formation of complex with the target metal ion. After filtration, the concentration of metal ions in the filtrate was determined by atomic absorption spectroscopy and by using a calibration curve made from standard solutions of metal salts. The amount of adsorbed ions was calculated using the following equation:

$$Q_t = \frac{[(C_0 - C_A) \times V]}{W} \quad (1)$$

where Q_t is the amount of metal ions adsorbed into the unit of the composites (mg g^{-1}), C_0 and C_A are the concentrations of metal ions in the initial solution and in the aqueous phase after adsorption, respectively (mg mL^{-1}), V is the volume of the initial solution (mL) and w is the weight of the polymer (g). Selectivity coefficient of adsorption of metal ions in the solution was studied in the mixture by batch procedure. The distribution coefficients (k_d) of ions were determined by the following equation (1):

$$K_d = \frac{[(C_0 - C_{A0}) \times V]}{C_A \times W} \quad (2)$$

The extraction selectivity, α , is the ratio of two distribution coefficients as shown in equation (2). The Hg^{II} cation was taken as the reference, as it has the highest distribution coefficient.

$$\alpha = \frac{K_{\text{dm}^{n+}}}{K_{\text{dHg}^{2+}}} \quad (3)$$

As the synthesized PAs are insoluble in water and showed highly moisture absorptive, therefore only PA3 and its composite with 20 wt% mNS (NCPA3-20%) has been used in solid–liquid extraction. Fig. 12 shows AFM images taken from surface of sample before and after adsorption of Hg^{2+} . The difference in these images which is observed by their appearance and the size of the particles (~ 25 nm and ~ 87 nm before and after metal ion adsorption, respectively) reveal that the surface of sample is fully covered with layer of adsorbed substance. The results for distribution coefficient and selectivity in the mixture of metal ions in solution are shown in Table 5. As can be seen in this table, the extraction level of these cations Hg^{2+} , Cd^{2+} , Ni^{2+} , Co^{2+} , Cu^{2+} , Cr^{3+} and Fe^{3+} by solid nanocomposite (NCPA3-20%) increased almost three times in comparison with the absorption level by PA3. This increase in the metal ions extraction can be suggested to be due to formation of network structure in the nanocomposite materials which raise the amount of entrapped metal ions inside the entangled macromolecular chains. Also, the selective adsorption of Hg^{2+} cation in the mixture solution of all cations is the highest which is similar with the results obtained for each ion individually. It is clear from the results, selectivity factor, that the quantitative separation of Hg^{2+} cation from the rest of the cations is possible. The extraction level of these cations especially mercury from aqueous media by the PAs and solid nanocomposite

phases, points to future applications in the fields of membrane preparation for cation transport, water decontamination and in sensing materials, among other applications.

4. Conclusions

The design and synthesis of novel thermally stable PAs with improved solubility based on unsymmetrical aromatic diamine-bisphenol containing beneficial heterocyclic ring such as imidazole was the main objective of this work. Therefore, an aromatic tetrafunctional compound containing both $-\text{NH}_2$ and $-\text{OH}$ groups was synthesized, characterized and used for preparation of PAs in direct selective polycondensation in IL/TPP without using NMP/Py/LiCl. These PAs with M_w in the range of 44,755–56,920 g/mol exhibited high thermal stability based on their T_g and $T_{10\%}$ values which varied from 188 °C to 325 °C and from 407 °C to 456 °C in air, respectively, depending on the rigidity of the polymer backbone. These results support that such a modification of the polymer structure can be used as an effective strategy for imparting fluorescence emission in the visible light region and enhancing the processability of aramids while maintaining the high thermal stability. These PAs with reactive hydroxyl groups in the backbone were also used in the preparation of chemically bonded reinforced composite materials with the surface modified NS. As compared with the pure PAs, the mNS/PAs nanocomposites are significantly strengthened by increasing the tensile strength and have an improved thermal stability. The solubility, thermal and tensile properties of the nanocomposites showed dependence on the amount of mNS particles. The results also demonstrated that these PAs and particularly their composite with mNS can act efficiently as chelating agent for heavy metal ions.

References

- [1] Zheng Z, Wu T, Zheng R, Wu Y, Zhou X. Catal Commun 2007;8(1):39.
- [2] Kokorin A. In: Ionic liquids: applications and perspectives. Rijeka, Croatia, India: InTech; 2011. Copyright ©, Janeza Trdine 9, 51000.
- [3] Wasserscheid P, Welton T. Ionic liquids in synthesis. KGaA, Weinheim: Wiley-VCH Verlag GmbH & Co; 2002.
- [4] Kubisa P. Prog Polym Sci 2004;29(1):3.
- [5] Kubisa P. Prog Polym Sci 2009;34(12):1333.
- [6] Vygodskii YS, Lozinskaya EI, Shaplov AS. Macromol Rapid Commun 2002;23(12):676.
- [7] Yoneyama M, Matsui Y. High Perform Polym 2006;18(5):817.
- [8] Vygodskii YS, Shaplov AS, Lozinskaya EI, Filippov OA, Shubina ES, Bandari R, et al. Macromolecules 2006;39(23):7821.
- [9] Vygodskii YS, Lozinskaya EI, Shaplov AS, Lyssenko KA, Antipin MY, Urman YG. Polym J 2004;45:5031.
- [10] Cassidy PE. Thermally stable polymer. New York: Dekker; 1980. [Chapter 4].
- [11] Hearle JW. High-performance fibres. Cambridge, England: Woodhead Publishing Ltd; 2001.
- [12] García JM, García FC, Serna F, de la Peña JL. Prog Polym Sci 2010;35(5):623.
- [13] Gaudiana RA, Minns RA, Sinta R, Weeks N, Rogers HG. Prog Polym Sci 1989;14(1):47.
- [14] Kricheldorf HR, Bohme S, Schwarz G. Macromolecules 2001;34(26):8879.
- [15] Liou GS, Hsiao SH, Ishida M, Kakimoto M, Imai Y. J Polym Sci Part A Polym Chem 2002;40(16):2810.
- [16] Liu YL, Li SH, Lee HC, Hsu KY. React Funct Polym 2006;66(9):924.
- [17] Chauveau E, Marestin C, Martin V, Mercier RG. Polymer 2008;49(24):5209.
- [18] Ghaemy M, Amini Nasab SM. Polym Adv Technol 2011;22(12):2311.
- [19] Ghaemy M, Amini Nasab SM. Polym J 2010;42(8):648.
- [20] Amini Nasab SM, Ghaemy M. J Polym Res 2011;18(6):1575.
- [21] Ghaemy M, Amini Nasab SM. React Funct Polym 2010;70(5):306.
- [22] Ghaemy M, Alizadeh R. Eur Polym J 2009;45(6):1681.
- [23] Ghaemy M, Masoumi A, Amini Nasab SM, Hassanzadeh M. J Appl Polym Sci 2013;127(4):3169.
- [24] Ghaemy M, Alizadeh R. React Funct Polym 2011;71(4):425.
- [25] Cerneaux S, Zakeeruddin SM, Pringle JM, Cheng YB, Grätzel M, Spiccia L. Adv Funct Mater 2007;17(16):3200.
- [26] Chen S, Sui J, Chen L, Pojman JA. J Polym Sci Part A Polym Chem 2005;43(8):1670.
- [27] Jin Q, Liao G, Feng X, Zhang X, Jian X. J Sol-Gel Sci Technol 2008;46(2):208.
- [28] Punyacharoennon P, Srikkulit K. J Appl Polym Sci 2008;109(5):3230.
- [29] Sinha Ray S, Okamoto M. Prog Polym Sci 2003;28(11):1539.

Table 5
Distribution coefficient (K_d) and selectivity (α) in competitive conditions.

Metal Cations	Distribution coefficient (K_d , mLg^{-1})		Selectivity factor (α)	
	NCPA3-20%	PA3	NCPA3-20%	PA3
Hg (NO_3) ₂	138.04	50.70	1.00	1.00
Cd (NO_3) ₂	49.29	10.66	0.36	0.22
Ni (NO_3) ₂	52.76	12.17	0.38	0.23
Co (NO_3) ₂	57.33	15.45	0.41	0.29
Cu (NO_3) ₂	64.21	16.88	0.46	0.33
Cr (NO_3) ₃	95.87	27.09	0.69	0.53
Fe (NO_3) ₃	73.65	21.22	0.53	0.41

- [30] Yu Y, Rong MZ, Zhang MQ. *Polymer* 2010;51(2):492.
- [31] Park HB, Kim JH, Kim JK, Lee YM. *Macromol Rapid Commun* 2002;23(9):544.
- [32] Van Zyl WE, García M, Schrauwen BA, Kooi BJ, De Hosson JT, Verweij H. *Macromol Mater Eng* 2002;287(2):106.
- [33] Luo Y, Rong MZ, Zhang MQ, Friedrich K. *J Polym Sci Part A: Polym Chem* 2004;42(15):3842.
- [34] Yamazaki N, Matsumoto M, Higashi F. *J Polym Sci Part A Polym Chem* 1975;13(6):1373.
- [35] Lozinskaya EI, Shaplov AS, Kotseruba MV, Komarova LI, Lyssenko KA, Antipin MY, et al. *J Polym Sci Part A Polym Chem* 2006;44(1):380.
- [36] Lu J, Yan F, Texter J. *Prog Polym Sci* 2009;34(5):431.
- [37] Lozinskaya EI, Shaplov AS, Vygodskii YS. *Eur Polym J* 2004;40(9):2065.
- [38] Hsiao SH, Chen CW, Liou GS. *J Polym Sci Part A Polym Chem* 2004;42(13):3302.
- [39] Ge Z, Yang S, Tao Z, Liu J, Fan L. *Polymer* 2004;45(11):3627.
- [40] Feng K, Hsu FL, Van DerVeer D, Bota K, Bu XR. *J Photoch Photobio A* 2004;165(1–3):223.
- [41] Liou GS, Chang CW. *Macromolecules* 2008;41(5):1667.
- [42] Van Krevelen DW, Nijenhuis KT. *Properties of polymers*. 4th ed. Amsterdam: Elsevier Scientific Publishing; 2008.